

Article

Creep and Hardening Characteristics of Anthracite under Graded Static–Dynamic Coupled Loading

Shaofei Yue^{1,2}, Kai Wang^{1,2,*} , Xiaoqiang Zhang^{1,2}, Tianhe Kang^{1,2}, Jianbing Yan^{1,2} and Yulong Jiang¹

¹ College of Mining Engineering, Taiyuan University of Technology, Taiyuan 030024, China; m18334705961@163.com (S.Y.); tyzxq2009@163.com (X.Z.); kangtianhe@163.com (T.K.); y20211013w@yeah.net (J.Y.); jiangyulong@tyut.edu.cn (Y.J.)

² Key Laboratory of In Situ Property-Improving Mining of Ministry of Education, Taiyuan 030024, China

* Correspondence: tywk2008@163.com

Abstract: Remaining coal pillars in remining areas exhibit clear creep characteristics, and dynamic pressure accelerates their instability and failure. The creep and hardening characteristics of coal under dynamic pressure are of great engineering significance for the stability of remaining coal pillars in remining areas and their control. To investigate the creep and hardening characteristics of anthracite under static–dynamic coupled loading, graded loading creep tests with different loading rates were conducted. In this research, the creep strain, instantaneous elastic modulus, and creep rate of anthracite were studied under different graded loading rates. The results showed that the hardening effect of the samples manifested as an increasing instantaneous elastic modulus at the loading stage and a decreasing strain rate at the creep stage. When the graded loading rate increases from 0.01 to 0.1 mm/s, the instantaneous elastic modulus increases by 0.16–2.32 times. The sudden increase in the instantaneous elastic modulus at the failure stress level explains the instantaneous failure of the samples well. The actual yield levels corresponding to the peak instantaneous elastic modulus of the samples linearly decreased with increasing graded loading rate. The functional relationship between the graded loading rate and the elastic modulus hardening coefficient, the actual yield stress, and the strain rate decay coefficient were established, which could quantitatively describe the influence of different graded loading rates on the creep and hardening characteristics of anthracite and predict its creep damage.



Citation: Yue, S.; Wang, K.; Zhang, X.; Kang, T.; Yan, J.; Jiang, Y. Creep and Hardening Characteristics of Anthracite under Graded Static–Dynamic Coupled Loading. *Appl. Sci.* **2023**, *13*, 10648. <https://doi.org/10.3390/app131910648>

Academic Editor: Tiago Miranda

Received: 22 August 2023

Revised: 20 September 2023

Accepted: 21 September 2023

Published: 25 September 2023



Copyright: © 2023 by the authors. Licensee MDPI, Basel, Switzerland. This article is an open access article distributed under the terms and conditions of the Creative Commons Attribution (CC BY) license (<https://creativecommons.org/licenses/by/4.0/>).

Keywords: graded loading creep; static–dynamic coupled loading; graded loading rate; hardening effect; creep characteristics

1. Introduction

Under the long-term action of roof pressure and mine water, the remaining coal pillars in remining areas exhibit clear rheological characteristics and their internal structures and mechanical parameters deteriorate to varying degrees [1,2]. Roadway excavation and working face mining in complex mining areas damage the original complex as well as the stable structure and stress environment. Notably, dynamic pressure accelerates the instability and failure of remaining coal pillars [3]. The creep characteristics of remaining coal pillars and their stability under dynamic pressure are important topics in the field of surrounding rock control in residual coal mining. Research has shown that loading rates considerably influence the damage and deformation patterns, mechanical parameters, and failure characteristics of coal or rock [4–6].

In coal, creep represents the process of the continuous development and adjustment of its internal structure with time; the failure and instability of coal result from the accumulation of damage and deformation in the internal structure. Establishing a nonlinear constitutive model to comprehensively reflect creep trends and characteristics is an important objective in engineering research. Researchers have conducted in-depth research on

creep characteristics and mechanisms [7–11]. Fan et al. [12] believed hardening to be the primary factor in dampening creep. The accumulation of internal damage in rocks leads to their deterioration and accelerates their creep. Wei et al. [13] explored the characteristics of creep curves for various elements by varying the fractional order and derived equations for the creep eigenstructure. Fahimifar et al. [14] concluded that the level of stress in materials substantially influences creep properties. Accordingly, they established a new creep model and verified its correctness through numerical simulations. Liang et al. [15] introduced the time hardening concept and derived a creep equation, further explaining the nature of nonlinear creep deformation. Song et al. [16] introduced the hardening stress threshold and hardening function and derived damage variables to establish a nonlinear creep model that could reflect the loading process. Zhang [17] considered the deterioration effect of creep and introduced a damage factor, which combined the damage evolution with time, intuitively reflecting the damage deterioration process of rocks. Zou et al. [18] introduced a hardening function and damage variable into a creep test of red sandstone under graded loading. They established a modified Kelvin model that could reflect the creep hardening damage mechanism. They believed the hardening and damage to be transitive and cumulative. Cai et al. [19] established a viscoelastic–plastic constitutive model for describing the hardening damage characteristics of lean coal and reported that hardening was dominant at low stress levels; damage gradually appeared upon reaching the stress threshold.

The response modes of coal–rock mass to external loads are different, and the loading mode, rate, and strength directly affect the damage evolution, deformation, and failure trend of coal–rock mass [20–23]. Most studies on loading rates focus on the effect of loading rates on the mechanical properties and failure characteristics of rocks [24,25]. Li et al. [26] revealed the multiscale damage evolution and energy dissipation law of rocks under repeated impact loads at different loading rates through dynamic compression tests. Wu et al. [27,28] conducted a medium strain rate compression test and found that with increasing loading rate, the compressive strength and elastic modulus of rocks increased. Guzev et al. [29] demonstrated that with increasing load frequency, the dynamic Young's modulus increases. Marolt et al. [30] investigated the prediction of the lifetime for rock-like material under axial static compression at various load levels, showing that specimens have shorter lifetimes under higher load levels. Sun et al. [31] performed rock burst simulation experiments on granite roadways under different loading rates. They suggested that an increase in the loading rate promoted the damage and destruction of surrounding rock in the roadways. Using the particle flow code platform, Wang et al. [32] found that the loading rate introduced a strengthening effect on the peak stress of a fractured body model. Gattu. [33] found that the loading rate influenced the fracture energy dissipation and the damage of limestone. Oh et al. [34] discussed the anisotropic effect on fracture toughness for granitic rocks at different loading rates. In terms of graded loading creep, Xin et al. [35] conducted post-peak incremental loading creep tests under different loading rates, revealing how the loading rates affect both the instantaneous and creep strains of rock samples. Wang et al. [36] performed uniaxial compression and acoustic emission tests on salt–rock samples under different loading rates. The test results showed that with increasing loading rates, the peak stress of the samples first increased and then remained unchanged. Moreover, the elastic modulus gradually increased, while the strain at the peak stress gradually decreased. Huang et al. [37] investigated the mechanical and creep properties of initially damaged coal samples under different loading rates. Their results showed that with increasing loading rates, the instantaneous strain first nonlinearly decreased and then increased, and the stress threshold first gradually decreased and then increased. Miyazaki et al. [38] quantitatively discussed the time-dependent properties of the methane hydrate bearing and considered the strong correlation between creep life and the loading rate. Li et al. [39] conducted a step-by-step incremental loading test that demonstrated the loading rate to be negatively correlated with the force adjustment time. Li et al. [40] and Fan [41] reported that with increasing loading rates, the creep deformation and rate gradually increased, and the creep rate of mudstone gradually attenuated with time.

The current studies mostly focus on the creep characteristics under static loading or mechanical characteristics under the dynamic loading of coal–rock, and few graded loading creep tests consider the effect of loading rate. Therefore, the present study conducted graded loading creep tests on anthracite samples under loading rates of 0.01–0.1 mm/s and analyzed the strain/strain rate evolution trend and hardening characteristics during the creep process. Moreover, it quantitatively investigated the effect of graded loading rates on the creep characteristics of anthracite coal. The research results can provide guidance for controlling the stability of remaining coal pillars under the influence of driving disturbance and mining dynamic pressure.

2. Methodology

2.1. Preparation and Treatment of Coal Samples

The samples of this study comprised anthracite coal No. 3 obtained from the Haitian Coal Industry in the Qinshui coal field, Jincheng City, Shanxi Province, North China. Water-saturated anthracite coal samples for conducting creep tests were prepared, described as follows:

- (1) Firstly, cylindrical coal samples with a size of $\phi 50 \text{ mm} \times 100 \text{ mm}$ were prepared with non-parallelism of less than 0.05 mm (Figure 1a), in accordance with the standards in the International Creep Principle and Hardening Mechanism (IRSM).
- (2) Then, to minimize the influence of the discreteness of the macro-mechanical properties of the samples on the test results, eight coal samples with similar density and longitudinal wave velocity (error less than 5%) were selected as the research objects in this test (Figure 1b).
- (3) Following this, the samples were dried in an oven at a constant temperature ($60 \text{ }^\circ\text{C}$) until the weight of the samples did not decrease according to GB/T23561.6-2009 (Figure 1c). Afterwards, the dry density of the samples was measured.
- (4) Thereafter, the samples were completely immersed in water for seven days until the weight of the samples did not increase and all the samples were saturated with water (Figure 1d). The wet density and water content of the water-saturated samples were measured.
- (5) After that, the porosity of the water-saturated samples was calculated based on a 3D pore-fracture map (Figure 1e), reconstructed based on CT scan results [42,43].

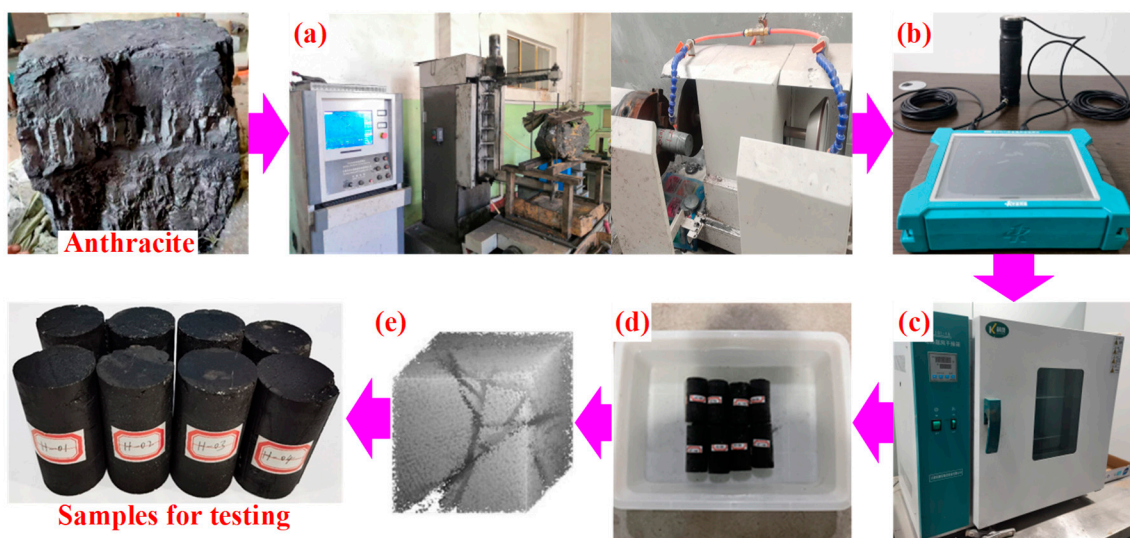


Figure 1. Anthracite sample preparation process. (a) Sample processed, (b) Wave velocity measurement, (c) Samples drying, (d) Samples water-saturated, (e) Porosity measurement.

Values of the mechanical properties of the anthracite coal samples are presented in Table 1.

Table 1. Values of the mechanical properties of anthracite coal samples.

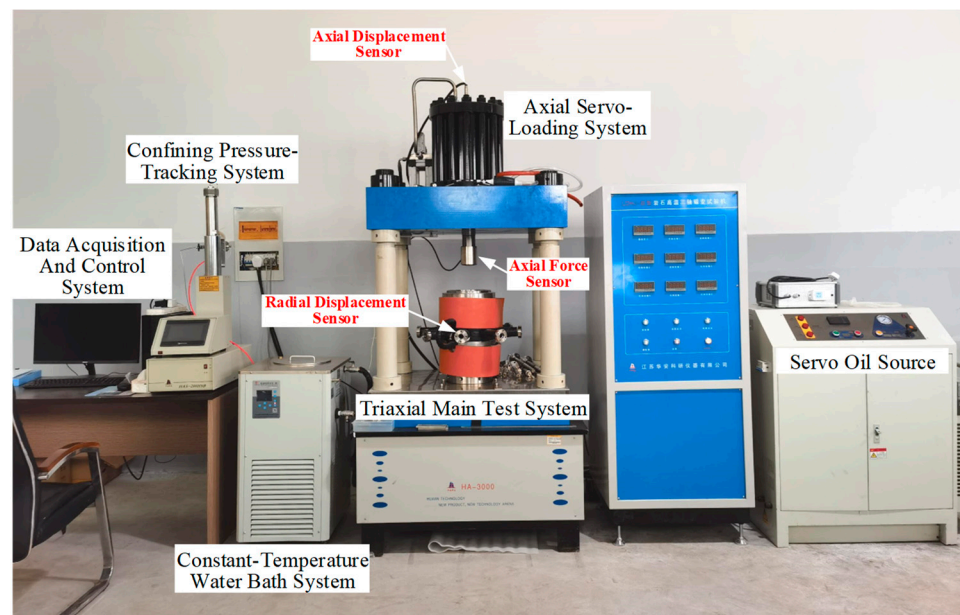
Parameter	Dry Density (g/cm ³)	Wet Density (g/cm ³)	Longitudinal Wave Velocity (m/s)	Porosity (%)	Water Content (%)
Measured value	1.43–1.51	1.47–1.56	1536.6–1742.8	6.87–10.54	2.95–3.52
Average value	1.46	1.51	1653.40	8.28	3.18
Standard deviation	0.02	0.03	50.35	0.94	0.18

In order to conduct conventional compression tests and graded loading creep tests, the samples obtained through the above steps were divided into two groups. The samples for the conventional compression tests are denoted as H-01, H-02, and H-03, and the samples for the graded loading creep tests are denoted as H-04, H-05, H-6, H-07, and H-08.

2.2. Test Equipment

The test was performed using an LDHJ-III rock high-temperature triaxial creep testing machine, independently designed and developed by our research group and Jiangsu Huaan Scientific Instrument Co., Ltd. The primary systems of the testing machine included a triaxial main test system, an axial servo-loading system, a confining pressure-tracking system, a constant-temperature water bath system, a room temperature control system, a radial deformation measurement system, and a data acquisition and PC-integrated control system. The main structure and test principle of the testing machine are shown in Figure 2. The testing machine could realize uniaxial/triaxial compression and creep tests of coal and rock under pore water pressure.

The testing machine had the characteristics of system stability and high measurement and control accuracy. The testing machine can realize the graded loading of different graded loading rates by controlling the axial loading rate (0~3 mm/s). The maximum axial force was 500 kN, and the load distinguishability was 0.01 kN. The radial deformation can be measured by eight displacement sensors around the sample. The axial and radial displacement distinguishability is 0.001 mm. The testing machine can well meet the requirements of this test. During the testing process, test pressure, axial and radial deformation, and temperature data could be recorded and plotted.

**(a)** Test machine**Figure 2.** Cont.

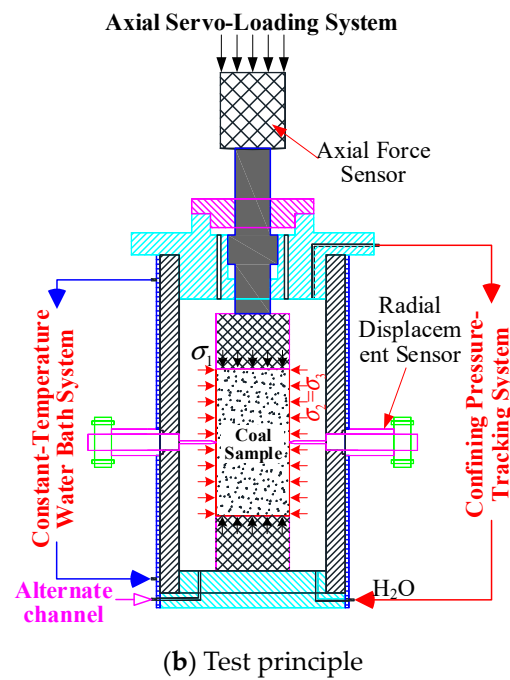


Figure 2. Schematic of the structure and principle of the testing machine.

2.3. Test Scheme and Steps

The basic mechanical parameters of the coal samples were determined before the creep test using conventional compression tests. These parameters served as the basis for determining the initial stress level and graded loading gradient in the creep test.

According to the strength characteristics of the samples, the initial stress level is 3 MPa, and the graded loading gradient is 1 MPa. An axial graded loading with different values was realized by controlling the displacement loading rate. The graded loading rate was set to 0.01–0.1 mm/s, while the corresponding strain rate was 10^{-4} – 10^{-3} /s. The scheme and process of the graded loading creep test were as follows. First, an axial and a confining pressure were simultaneously applied with predetermined values to put the sample under hydrostatic pressure. Then, an axial stress was applied step-by-step until it reached the target level according to the loading scheme. The axial stress was kept constant for >24 h. Subsequently, axial stress was applied to the next stage. Finally, the above graded loading creep process was repeated until the sample was damaged. The axial and radial stresses and the deformation data were recorded during the test. The confining pressure was 2 MPa and the testing temperature was 25 ± 0.5 °C, remaining constant during the test.

The loading scheme of each sample is summarized in Table 2, and the graded loading method and path of the creep test are presented in Figure 3.

Table 2. Sample loading scheme.

Sample Number	Type of Test	Graded Loading Rate V_l (mm·s ⁻¹)	Graded Loading Strain Rate $\dot{\epsilon}_l$ (s ⁻¹)	Axial Loading Path (MPa)
H-01–H-03	Conventional compression test	0.002	2×10^{-5}	Apply axial stress until the sample is damaged.
H-04	Graded loading creep test	0.01	10^{-4}	3→4→5→6→7→8 →9→10→11→12→13
H-05		0.02	2×10^{-4}	
H-06		0.04	4×10^{-4}	
H-07		0.06	6×10^{-4}	
H-08		0.1	10^{-3}	

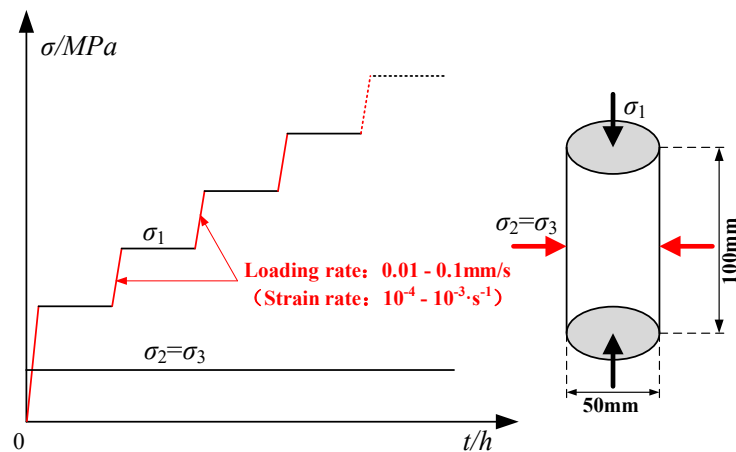


Figure 3. Schematic of the graded loading path for creep tests.

2.4. Creep Principle and Hardening Mechanism

Researchers have found that not only the damage and softening effects but also the hardening effect occur during the creep process of coal and rock mass [15–19]. The damage effect and the hardening effect restrict the development of each other and act during the entire creep process. The damage effect primarily manifests as the continuous deterioration of the sample, which can well explain the continuous increase in the strain and the generation of accelerated creep. The hardening effect primarily manifests as a gradual increase in the ability of the sample to resist deformation under an external load, which can well explain the generation of decay creep. The effect of the creep hardening of the sample can be quantified using the elastic modulus [44]. Under graded loading, the damage degree of the samples varies with the stress level, and the elastic modulus exhibits a clear timeliness at different loading levels. The hardening effect is directly reflected in the increase in the instantaneous elastic modulus and strain during the graded loading stage. After the samples are damaged owing to continuous creep and loading, the decay creep characteristics in the creep stage can also reflect the hardening characteristics of the samples. In a subsequent test, the influence of different graded loading rates on the creep-hardening effect of anthracite coal was studied based on three aspects: the strain increment in the loading stage, instantaneous elastic modulus hardening in the loading stage, and strain rate attenuation in the creep stage.

During the creep test, axial stress was applied to the sample via graded loading (Figure 3). At the i th stress, the stress remains constant, and the strain increases with time. The diagram of stress and strain with time is shown in Figure 4.

The generated strain has two components at each stress level: the instantaneous and creep strains. The relation among the increments of these strains at each stress level can be expressed as follows:

$$\Delta \varepsilon_i = \Delta \varepsilon_{i1} + \Delta \varepsilon_{i2}, \tag{1}$$

where $\Delta \varepsilon_i$, $\Delta \varepsilon_{i1}$, and $\Delta \varepsilon_{i2}$ indicate the increments in the total, instantaneous, and creep strains at the i th stress level, respectively.

During the loading stage, the axial stress increases from σ_{i-1} to σ_i , and the instantaneous elastic modulus of a sample can be obtained as follows:

$$E_i = \Delta \sigma_i / \Delta \varepsilon_{i1}, \tag{2}$$

where E_i , $\Delta \sigma_i$, and $\Delta \varepsilon_{i1}$ are the instantaneous elasticity modulus of the sample, the stress increment, and the instantaneous strain increment, respectively, at the i th stress level.

To quantitatively express the influence degree and trend of the graded loading rate on the hardening effect for a sample, in this experiment the elastic modulus hardening coefficient K can be defined as follows:

$$K = E_i / E_c \tag{3}$$

$$E_c = \Delta\sigma / \Delta\varepsilon, \tag{4}$$

where E_i is the instantaneous elastic modulus of the sample at the i th stress level, E_c is the elastic modulus in the conventional compression tests, and $\Delta\sigma$ and $\Delta\varepsilon$ are the stress and strain increments in the linear elasticity phase in the conventional compression tests.

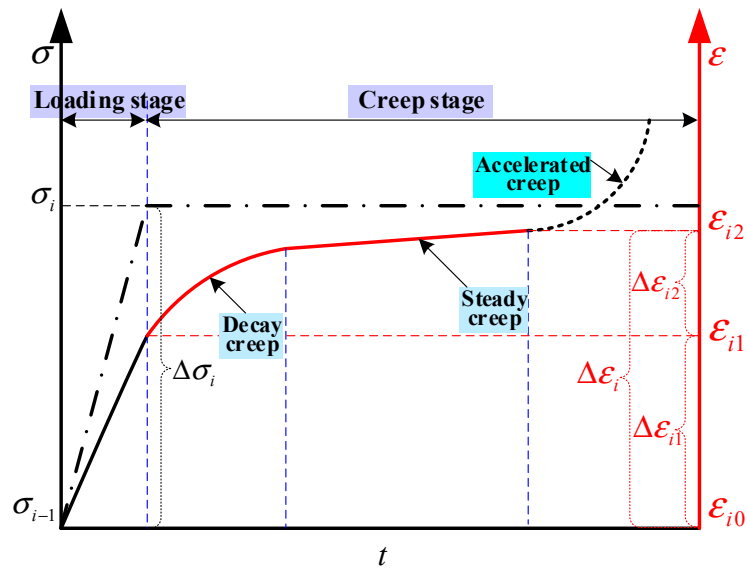


Figure 4. Principle of graded loading creep test.

During the creep stage, the creep rate constantly decays and shows a “decreasing–stabilizing” trend, which is called the decay creep and steady creep stage, respectively. The evolution of the creep rate and strain of the sample in the creep stage is shown in Figure 5.

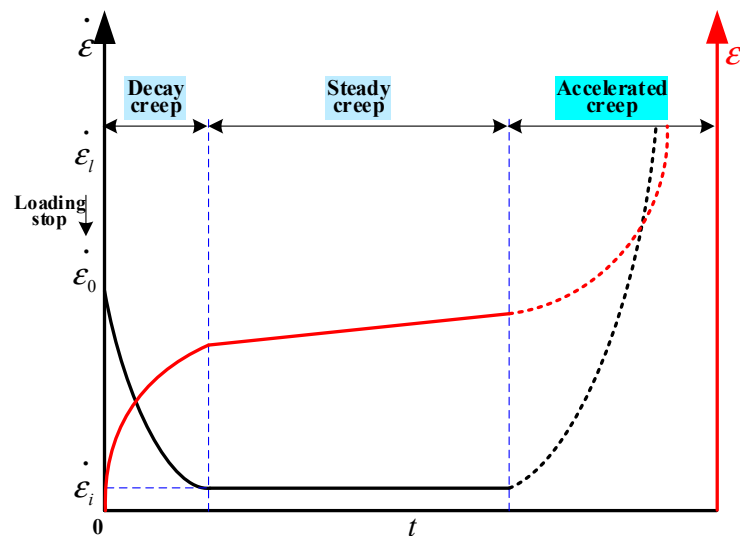


Figure 5. Diagram of creep rate evolution during creep stage.

In order to investigate the creep rate decay characteristics of the sample at the initial moment of the creep stage, in this experiment, we define the strain rate decay coefficient A at the initial moments of the creep stage, which can be obtained as follows:

$$A = 1 - \frac{\dot{\varepsilon}_0}{\dot{\varepsilon}_l}, \quad (5)$$

where $\dot{\varepsilon}_0$ is the strain rate at the initial moments of the creep stage and $\dot{\varepsilon}_l$ is the axial loading strain rate given in Table 2.

3. Results

3.1. Conventional Compression Test Results

The main mechanical parameters of three samples (H-01–H-03) are given in Table 3. Under conventional compression test conditions, the peak strength of these three samples was 13.211–13.485 MPa, while their axial and radial peak strains were 0.9698–1.1126% and 1.054–1.139%, respectively. The stress–strain curve of the samples (Figure 6) comprised three typical stages: the compaction, linear elasticity, and yield failure stages.

Table 3. Triaxial compression mechanical parameters of anthracite samples.

Sample Number	H-01	H-02	H-03	Average
Peak strength (MPa)	13.184	13.485	13.211	13.293
Axial peak strain (%)	0.9949	0.9698	1.126	0.9733
Radial peak strain (%)	1.139	1.054	1.187	1.127
Elastic modulus (MPa)	1803.6	1895.1	1606.1	1768.3
Poisson's ratio	0.32	0.36	0.29	0.323

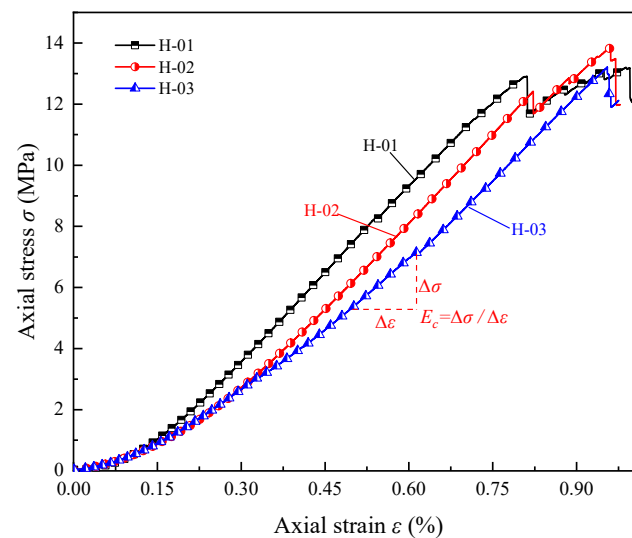


Figure 6. Strain–time curves for the conventional compression test.

Figure 6 shows that when the stress was <5 MPa, the sample deformation exhibited clear nonlinear characteristics, the stress–strain curve was downward concave, and the instantaneous elastic modulus of the sample exhibited an increasing trend with increasing stress. During the compaction stage, when the stress was 5–10 MPa, the stress–strain curve was linear, the sample was elastically deformed, and the average elastic modulus of the coal sample was 1768.3 MPa. When the stress was >10 MPa, the stress–strain curve was upward convex, and the instantaneous elastic modulus of the sample gradually became smaller with increasing stress. Moreover, as the sample entered the yield failure stage, new cracks formed inside the coal sample, and the deformation further developed. When the stress exceeded 12 MPa, the sample showed a clear internal structure adjustment and a

small pressure drop occurred, followed by an internal crack. Failure occurred when the stress increased and reached the value of the peak failure stress.

3.2. Graded Loading Creep Test Results

After collecting the strain data of the H-04–H-08 samples, the sample strain–time curves were obtained (Figure 7). The trends of the strain–time curves of all these samples were similar for the entire creep process. When the stress level was less than or equal to 11 MPa, the samples experienced two stages of decay creep→steady creep and they remained stable after 24 h of creep. When the stress level was 12 MPa, all five samples were destroyed, and compared with the conventional compression test, the failure strength of the samples in the creep test decreased by 9.73%. This phenomenon occurs due to the damaging effect of the graded loading and accumulation of multilevel creep damage. Notably, the H-04–H-06 samples experienced three stages of attenuated creep→steady creep→accelerated creep under a 12 MPa stress level. However, the H-07 and H-08 samples directly entered the stage of accelerated creep after a 12-MPa stress loading was completed; they rapidly destabilized and experienced failure. The instantaneous failure characteristics of the H-07 and H-08 samples were clear. The strength and strain parameters of the H-04–H-08 samples are given in Table 4.

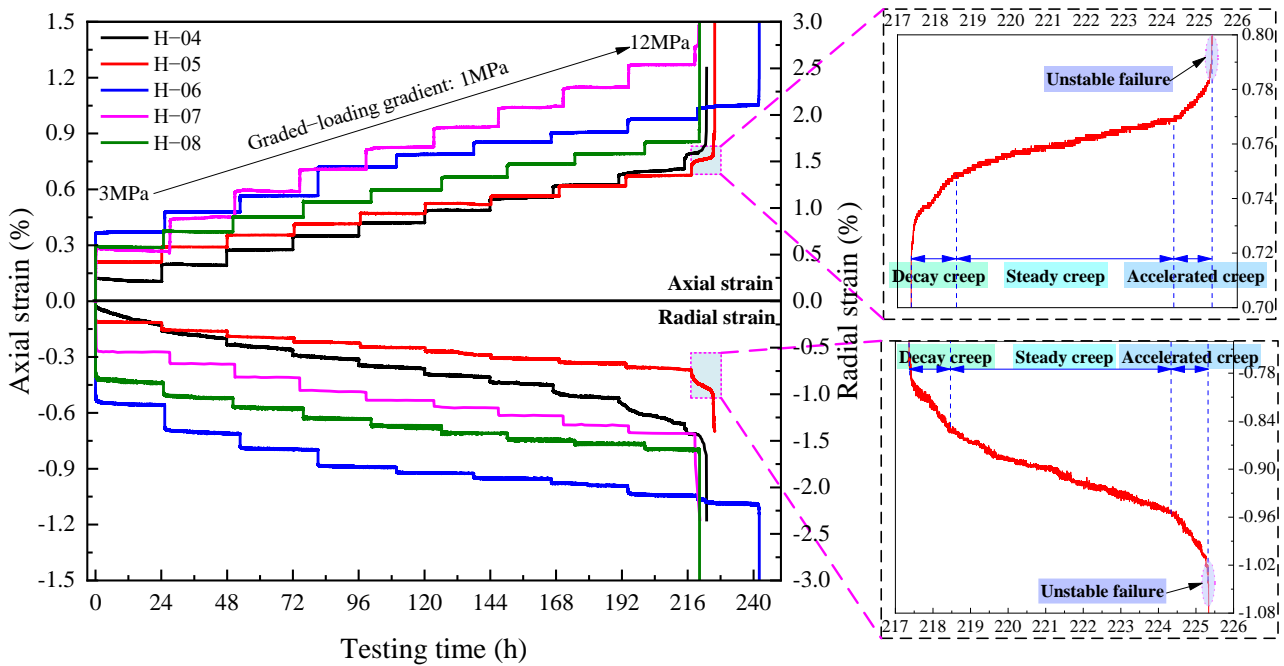


Figure 7. Strain–time curves for the entire creep process.

Table 4. Strain parameters of the H-04–H-08 samples.

Sample Number	Graded Loading Rate V_l (mm·s ⁻¹)	Axial Peak Strain		Radial Peak Strain	
		Value (%)	Compared with That in the Conventional Compression Test (%)	Value (%)	Compared with That in the Conventional Compression Test (%)
H-04	0.01	1.259	+22.23	1.352	+31.65
H-05	0.02	1.308	+26.99	1.404	+46.45
H-06	0.04	1.428	+38.64	2.383	+132.04
H-07	0.06	1.256	+21.94	1.856	+80.72
H-08	0.1	1.059	+2.82	1.665	+62.12

Table 4 indicates that compared with those in the conventional compression test, the axial peak strain increased by 2.82–38.64%, and the radial peak strain increased by

31.65–132.04% in the creep test. With increasing graded loading rates, the axial and radial peak strains of the samples first increased and then decreased. The increase in the radial strain was more than that in the axial strain. Based on the combination of these results with the failure characteristic analysis results for each sample, the samples in the creep test were believed to experience cracks under the graded loading. Under a long-term creep action, more cracks were generated inside the samples and continued to develop and expand, and the internal structure clearly expanded and became damaged. The radial strain of the samples increased more considerably than the axial strain, indicating that the radial expansion caused by the development and expansion of cracks in the samples clearly occurred during the creep process. Although the failure strengths of the samples were the same under different loading rates, the failure times, failure trends, and deformation conditions were different. In particular, the strain of the samples was considerably correlated with their loading rate.

4. Discussion

4.1. Relation between the Strain Increment at Each Stress Level and Graded Loading Rate

In order to investigate the effect of loading rate on sample strain, the strain increments of the samples at each stress level were analyzed. The composition of the strain increments at each stress level substantially differs for different graded loading rates (Table 5). The variation in the proportion of the instantaneous strain increment with the graded loading rate is depicted in Figure 8.

Table 5. Proportion of the instantaneous strain increment at each stress level in the total strain increment.

Sample Number	Graded Loading Rate V_l ($\text{mm}\cdot\text{s}^{-1}$)	$\Delta\varepsilon_{i1}/\Delta\varepsilon_i$ (%) (Axial)		$\Delta\varepsilon_{i1}/\Delta\varepsilon_i$ (%) (Radial)	
		Minimum–Maximum	Average	Minimum–Maximum	Average
H-04	0.01	57.69–73.85	66.54	8.85–12.92	9.58
H-05	0.02	52.96–66.61	59.27	7.12–16.03	10.77
H-06	0.04	33.33–56.74	46.72	11.95–25.67	16.94
H-07	0.06	25.54–56.15	34.56	8.65–75.58	39.57
H-08	0.1	6.15–58.53	28.64	4.90–84.56	65.24

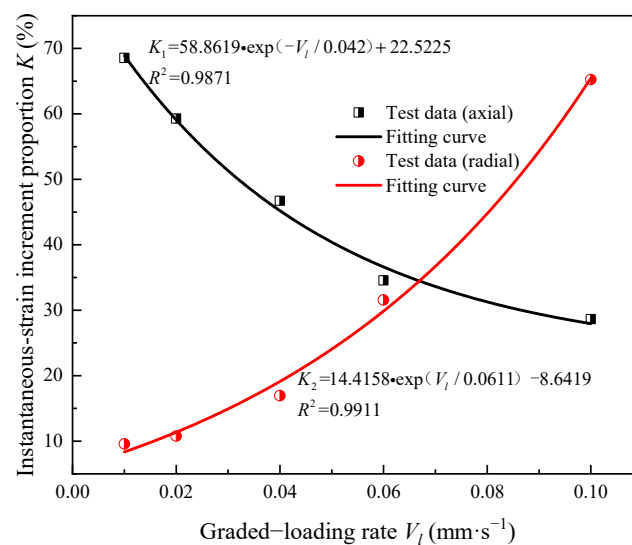


Figure 8. Relation between the instantaneous strain increment proportion and the graded loading rate.

The sensitivities of the axial and radial strains to the loading are characterized based on the percentage of the instantaneous strain increments to the total strain increments

to quantitatively explain the effect of the graded loading rates on the strain increments. Figure 5 shows that these sensitivities and the graded loading rate exhibit an exponential relation. When the graded loading rate is <0.04 mm/s, the axial strain is dominated by the instantaneous strain, and the radial strain is dominated by the creep strain. Moreover, the radial strain exhibits clear hysteresis. With increasing loading rates, the sensitivities of the axial and radial strains to the loading decrease and increase, respectively. When the loading rate is increased from 0.01 mm/s to 0.1 mm/s, the sensitivity of the axial strain decreases from 66.54% to 28.64%, while that of the radial strain increases from 9.58% to 65.24%.

A comprehensive analysis shows that with increasing graded loading rate, the sensitivity of the axial strain to the axial loading gradually decreases. Moreover, the axial strain generated by the samples during the loading stage decreases. The axial strain hysteresis effect gradually becomes clear. The sensitivity of the axial strain to the loading shows the most reduction in the linear elasticity stage. Moreover, it exhibits a linear relation with the hierarchical graded loading rate, indicating that the ability of the sample to resist deformation in the linear elasticity stage rapidly increases with increasing graded loading rate, and the hardening characteristics of the samples become clear. The overall sensitivity of the radial strain to the loading exhibits an increasing trend, and the macroscopic performance indicates that the radial expansion of the sample during the loading stage is clear, especially when the graded loading rate is >0.04 mm/s. The sensitivity of the radial strain to the axial loading is considerably improved with increasing graded loading rate. The results reflect that the axial and radial strains of the samples during the creep process show obvious asynchrony, and the radial strain shows obvious hysteresis, which was also proved in the literature [19].

4.2. Evolution Trend of the Instantaneous Elastic Modulus in the Loading Stage

In this section, the instantaneous elastic modulus evolution law of the samples during the creep test is investigated. Moreover, the hardening effect of the samples under different graded loading rates was analyzed. The variation in the instantaneous elastic modulus with the stress level at different loading stages under the same stress gradient conditions is depicted in Figure 9. The boxplots of the instantaneous elastic modulus under different graded loading rates are presented in Figure 10.

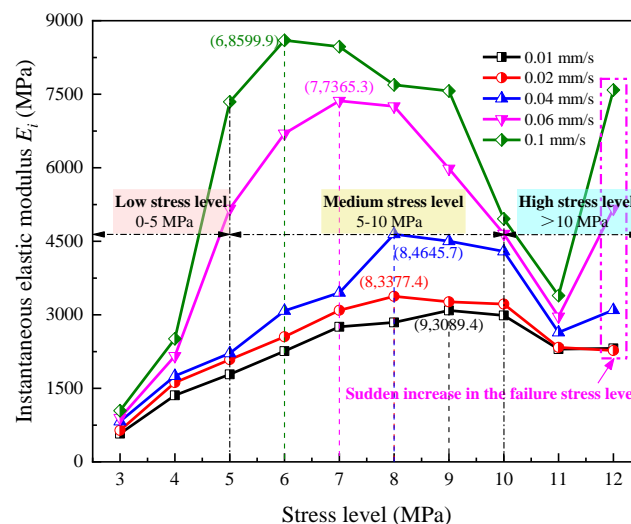


Figure 9. Variation in the instantaneous elastic modulus with the stress level.

Figure 9 shows that at the initial stress level, the elastic modulus of each sample is 574.6–1042.98 MPa. The hardening effect is mainly reflected in the medium stress level. The elastic moduli of the samples are the largest at this stage, and the hardening effect is the most clear. Figures 6 and 7 show that the instantaneous elastic modulus at each stress level shows increases with increasing graded loading rate. When the graded loading rate increases

from 0.01 to 0.04 mm/s, the instantaneous elastic modulus increases by 0.15–0.63 times (average: 0.36). However, when the graded loading rate increases from 0.04 to 0.1 mm/s, the instantaneous elastic modulus is considerably affected and increases by 0.16–2.32 times (average: 0.95), and the hardening effect is considerably enhanced. Zou et al. [18] analyzed the hardening effect of red sandstone under graded loading creep conditions and showed that the instantaneous elastic modulus first increases and then decreases with increasing stress levels, indicating a good agreement with this study.

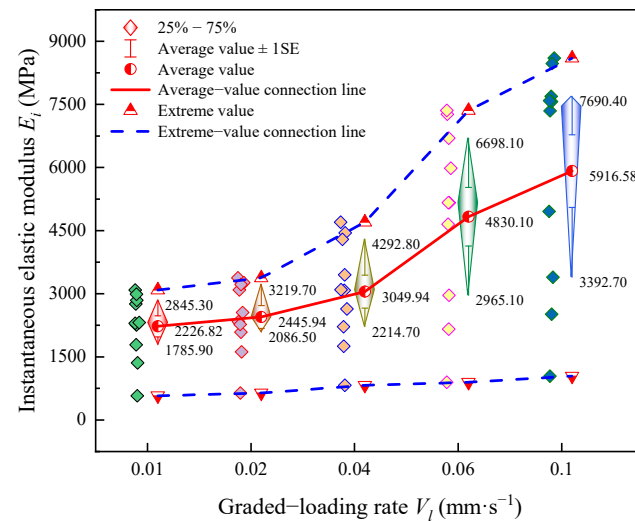


Figure 10. Boxplots of the instantaneous elastic modulus.

Figure 10 shows that with increasing graded loading rate, the discreteness of the elastic moduli of the samples in the entire hierarchical creep process increases. The macroscopic performance shows that the heterogeneity of the entire creep process for the samples is clearly enhanced under the graded loading.

From the perspective of the entire creep process, we can observe that at a low stress level (0–5 MPa), the graded loading rate has little effect on the instantaneous elastic moduli, mainly because the samples are in the compaction stage. The continuous adjustment of the internal primary fractures and mineral units exerts a clear buffering effect on the external loads. The instantaneous elastic modulus is not sensitive to the graded loading rate but exhibits an overall increasing trend. The growth rates of the elastic moduli of the H-07 and H-08 samples are considerably higher than those of the other samples. Under a medium stress level (5–10 MPa), the samples are theoretically in the linear elasticity stage and the elastic moduli remain unchanged. However, under the influence of the graded loading rate, the instantaneous elastic moduli of the samples gradually increase and the effect of elastic energy accumulation inside the samples gradually becomes notable. At this stage, the sample deformation primarily corresponds to elastic deformation. As per the results presented in Figure 9, the sample strain exhibits a decreasing trend with the stress level, and the hardening effect of the samples is clear. Especially, when the graded loading rate is >0.04 mm/s, the instantaneous elastic modulus and its growth rate are considerably larger than those of the other samples, and the hardening effect caused by the increase in the graded loading rate becomes clearer. After the stress level exceeds 10 MPa, the samples theoretically enter the yield failure stage. The continuous generation and expansion of internal cracks lead to a rapid decrease in the elastic modulus of the samples, and they gradually suffer from plastic failure. At this time, the sample strain increases and the damage degradation effect dominates.

The stress levels corresponding to the peak instantaneous elastic moduli of the various samples are 9, 8, 8, 7, and 6 MPa. After the respective stresses exceed these values, the instantaneous elastic moduli exhibit a decreasing trend in the loading stage and the ability of the samples to resist deformation weakens. The instantaneous strains of the samples in

the loading stage considerably increase, and the damage to the sample’s internal structure becomes notable. Herein, the stress corresponding to the peak value of the instantaneous elastic modulus is considered a critical value for the samples when entering the yield failure stage. With increasing graded loading rates, the actual yield stresses of the samples linearly decrease (Figure 11), and the samples become more prone to yield failure.

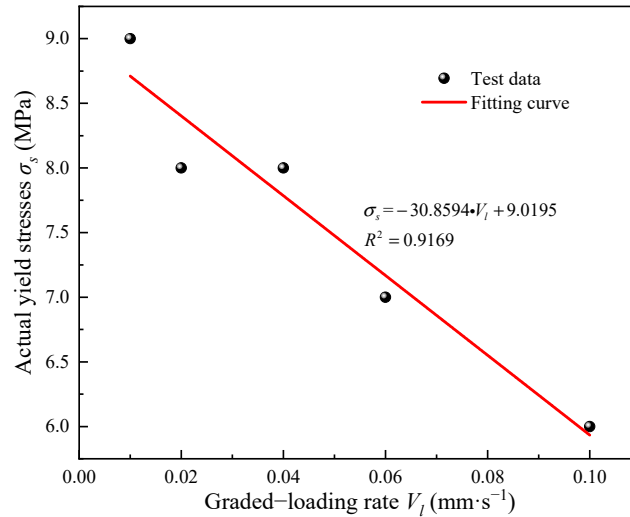


Figure 11. Actual yield stress versus the graded loading rate.

In order to analyze the hardening characteristics of the samples in a comprehensive way, we calculated the average hardening coefficient, the peak hardening coefficient, and the failure stress level hardening coefficient separately. The calculation results for the elastic modulus hardening coefficient K in the creep test are summarized in Table 6. The fitting relation of K with the graded loading rate is depicted in Figure 12.

Table 6. Relation between the hardening coefficient and graded loading rate.

Hardening Coefficient K	Graded Loading Rate V_l (mm·s ⁻¹)					Fitting Relation
	0.01	0.02	0.04	0.06	0.1	
Average value	1.259	1.383	1.725	2.731	3.346	$K_A = 24.858 \cdot V_l + 0.9455, R^2 = 0.9404$
Peak value	1.747	1.910	2.627	4.165	4.863	$K_P = 37.6204 \cdot V_l + 1.332, R^2 = 0.9203$
Failure stress level	1.310	1.285	1.751	2.921	4.291	$K_F = 35.4575 \cdot V_l + 0.6804, R^2 = 0.9551$

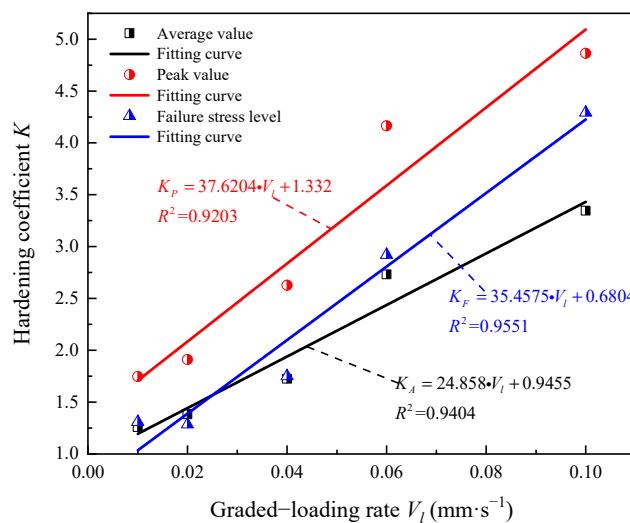


Figure 12. Relation between the elastic modulus hardening coefficient and graded loading rate.

As can be seen from Figure 12, K and the graded loading rate exhibit an increasing linear relation, and the growth trends of the peak and failure stress levels are similar.

Notably, at the failure stress level (12 MPa), the hardening effect of the sample is temporarily enhanced compared with that in the previous stress level (11 MPa) (Figure 9). In particular, the instantaneous elastic moduli of the H-07 and H-08 samples abruptly increase. To express the mutation of the elastic modulus at the failure stress level, the elastic modulus mutation coefficient K_n can be defined as follows:

$$K_n = E_n / E_{n-1}, \quad (6)$$

where E_n and E_{n-1} are the elastic moduli at the failure stress level and the stress level before failure, respectively. The values of K_n for each sample are calculated to be 1.007, 0.973, 1.173, 1.174, and 2.236. The fitting relation of the elastic modulus mutation coefficient (K_n) with the graded loading rate (V_l) is depicted in Figure 13.

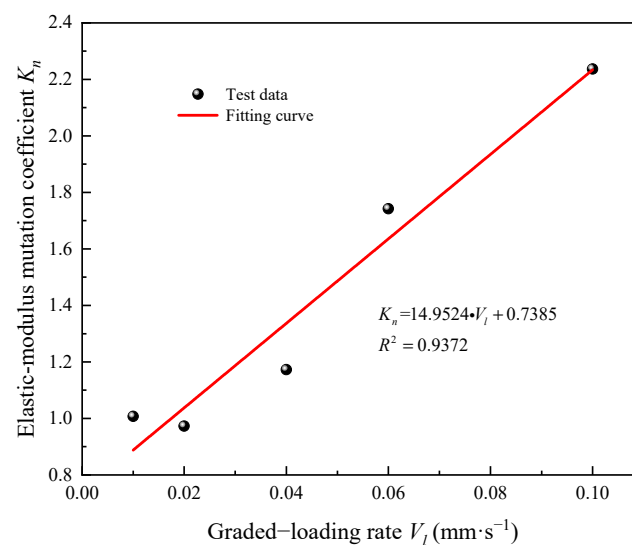


Figure 13. Abrupt change in the mutation coefficient of the elastic modulus (failure stress = 12 MPa).

It can be clearly observed from Figure 13 that the mutation coefficient of the elastic modulus at the failure stress level linearly increases with the graded loading rate. With increasing graded loading rates, the mutation of the hardening effect becomes more clear before the samples are destroyed. In particular, for the H-07 and H-08 samples, their elastic moduli at the failure stress level show a clear abrupt change; a large amount of energy is rapidly accumulated during the loading stage. The abrupt increase in the elastic moduli well explains the transient failure characteristics of the H-07 and H-08 samples.

According to the aforementioned analysis results, the graded loading rate directly affects the instantaneous elastic modulus of the samples during the loading stage. The hardening effect of the samples at medium–high stress levels is most sensitive to the graded loading rate; this is primarily reflected after the graded loading rate exceeds 0.04 mm/s. Under the failure stress, the hardening effect shows a tendency to increase compared with that at the stress level before failure. The macroscopic performance reveals that the sample strain considerably reduces in the loading stage. In the creep test, the creep failure of the samples can be predicted according to this phenomenon.

4.3. Characteristics of Strain Rate Decay in the Creep Stage

This subsection focuses on the strain rate decay and evolution characteristics of different samples during the creep stage and then analyzes the hardening characteristics of the samples. At different stress levels, each sample experiences the decay and steady creep stages. By employing the Origin software to smooth the strain–time curve and derive the strain, the creep rate–time curve can be obtained. By analyzing the strain/strain rate–time

curves of the H-04–H-08 samples in the creep stage, we can conclude that both the axial and radial strains exhibit a trend of rapid increase–slow increase–gradual stability. With increasing graded loading rate, the curvature of the strain–time curve increases and the transition of the strain becomes clearer with time. The strain rates also exhibit a trend of rapid decrease–slow decrease–gradual stability, with the initial creep rate being directly related to the graded loading rate.

Taking the 8 MPa stress level as an example, Figure 14 depicts the relation between the strain rate decay coefficient and axial-loading rate during the initial moments of the creep stage and the corresponding fitting curves.

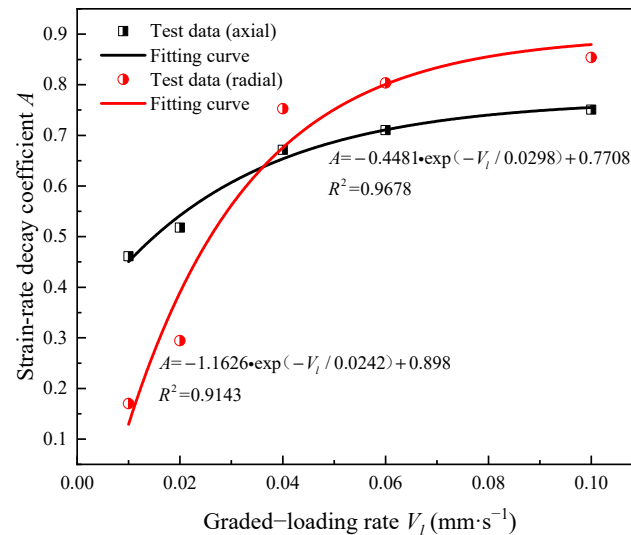


Figure 14. Relation between the strain rate decay coefficient and graded loading rate during the initial moments of the creep stage.

The axial and radial strain rates suddenly decrease upon stopping the loading. With an increasing strain rate attenuation coefficient at the initial creep moment, the magnitude of the sudden decrease in the strain rates increases. This indicates that the creep strain is more sensitive to the graded loading rate. Figure 14 shows that the initial strain rate attenuation coefficient and graded loading rate exhibit an exponential relation. When the graded loading rate increases from 0.01 to 0.1 mm/s, the attenuation of the initial axial strain rate increases from 46.1% to 75.1% and that of the initial radial strain rate increases from 17.0% to 85.4%. With increasing graded loading rates, the strain rate decay characteristics of the samples are considerably enhanced upon stopping the loading, and the radial strain rate decay is more affected by the graded loading rate in the axial direction. When the graded loading rate is >0.04 mm/s, the increasing trend of the curve (Figure 14) becomes slower and the effect of the graded loading rate on the strain rate decay coefficient considerably weakens during the creep stage.

By analyzing the creep rates of different samples, the creep rate is found to rapidly decay from 0 to 10 s, and the decay characteristics vary significantly between samples. Taking the 8 MPa stress level as an example, the relation between the time of the decay creep stage and the graded loading rate for different samples is shown in Figure 15, and the variation of the stable creep rate with the stress level at different loading rates is depicted in Figure 16.

Figure 15 shows that the time of the axial and radial strain decay creep stage of the various samples are 89 s, 68 s, 47 s, 42 s, and 37 s, and 92 s, 66 s, 53 s, 49 s, and 46 s, respectively. From the results, it is clear that the time of the decay creep stage decreases with increasing graded loading rates, which indicates that the strain rate decay due to hardening effects is notable. Moreover, the time for the radial strain is longer than that for the axial strain; the radial strain indicates clear hysteresis. A similar conclusion was reached in the literature [19].

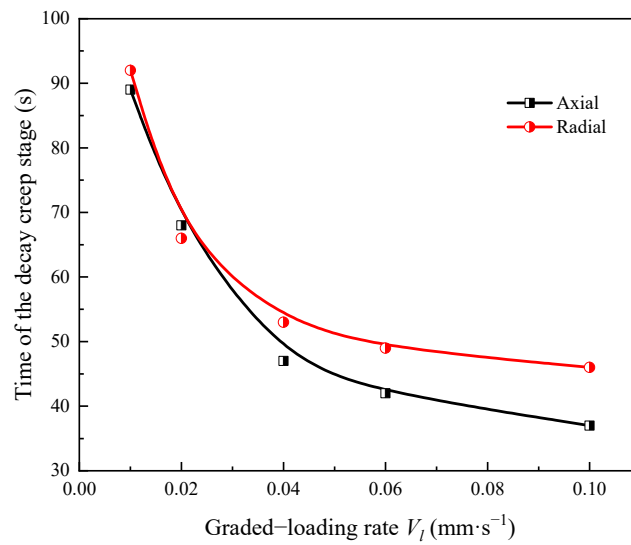


Figure 15. Relation between the time of the decay creep stage and the graded loading rate.

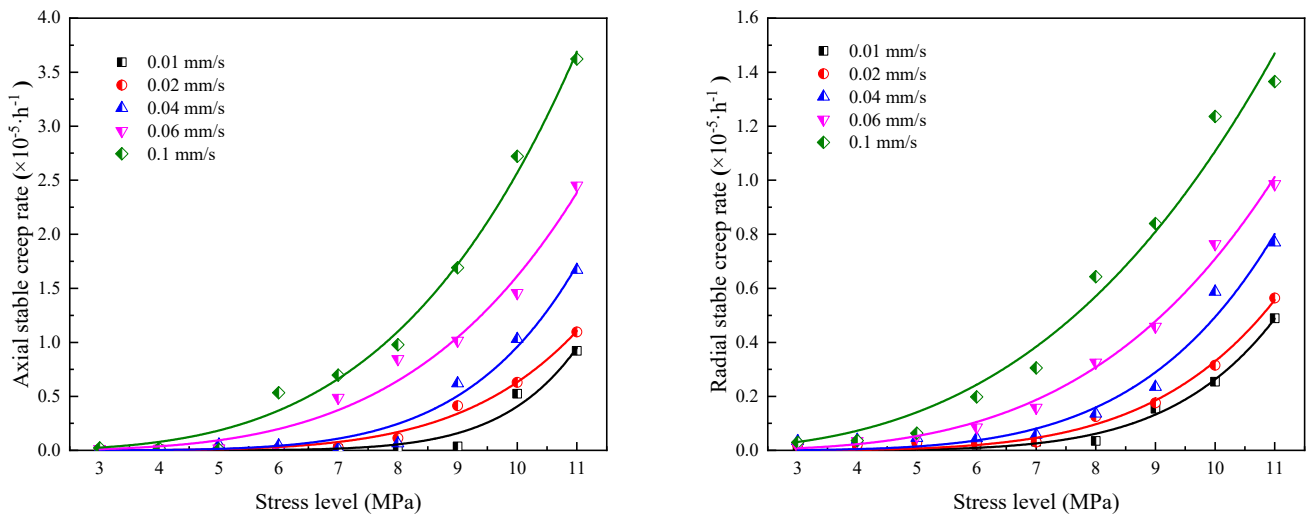


Figure 16. Variation of the stable creep rate with the stress level.

It can be clearly observed from Figure 13 that the stable creep rate of samples at each stress level shows a nonlinear increasing trend. When the stress level is over its actual yield stress (Figure 16), the stable creep rate increases significantly, indicating that the damage effect of the sample in the creep stage is enhanced. At the same stress level, the stable creep rate shows an increasing trend with increasing graded loading rates.

5. Conclusions

By performing creep tests under different graded loading rates (0.01–0.1 mm/s), the effects of graded loading rates on the creep and hardening characteristics of anthracite were explored. The results revealed the mechanical properties of remaining coal pillars under dynamic pressure, providing a basis for their stability determination. The conclusions obtained from this study can be summarized as follows.

- (1) The hardening effect of the sample prepared in this study manifested as increasing instantaneous elastic modulus at the loading stage and decreasing strain rate at the creep stage.
- (2) The graded loading rate directly affects the instantaneous modulus of elasticity of the samples. With stress level increasing, the instantaneous elastic modulus at each stress level exhibited an increase–decrease–increase trend. The actual yield levels

- corresponding to the peak instantaneous elastic moduli of the samples are 9, 8, 8, 7, and 6 MPa, which linearly decreased with increasing graded loading rates.
- (3) With graded loading rates increasing from 0.01 to 0.1 mm/s, the instantaneous elastic modulus increases by 0.15–2.63 times, the elastic modulus hardening coefficient and the graded loading rate exhibit an increasing linear relation; when the graded loading rate was >0.04 mm/s, the hardening effect was considerably enhanced.
 - (4) The hardening effect of the elastic modulus of the samples abnormally increased at the failure stress level compared with that at the previous stress level. With increasing graded loading rates, the mutation coefficient increased from 1.007 to 2.236, which linearly increased with increasing graded loading rates. When the graded loading rate was >0.04 mm/s, the sudden increase in the instantaneous elastic modulus resulted in a rapid accumulation of elasticity energy, which well explains the instantaneous failure and instability of the samples.
 - (5) The initial strain rate attenuation coefficient and graded loading rate exhibit an exponential relation. With increasing graded loading rates, the attenuation of the initial axial strain rate increases from 46.1% to 75.1%, and that of the initial radial strain rate increases from 17.0% to 85.4%. Moreover, the time of the decay creep stage for the radial strain is longer than that for the axial strain; the radial strain indicates clear hysteresis.

Author Contributions: S.Y.: Writing—Original Draft, Data Curation, Methodology, Formal analysis. K.W.: Methodology, Supervision. X.Z.: Methodology Supervision. T.K.: Writing—Review and Editing. J.Y.: Data Curation. Y.J.: Methodology Supervision. All authors have read and agreed to the published version of the manuscript.

Funding: This research was funded by [National Natural Science Foundation of China] grant number [51974194, 51704204].

Institutional Review Board Statement: Not applicable.

Informed Consent Statement: Not applicable.

Data Availability Statement: The datasets used and/or analyzed during the current study are available from the corresponding author on reasonable request.

Acknowledgments: The authors would like to appreciate the financial support from the National Natural Science Foundation of China [Grant No. 51974194, 51704204]. Thanks to all co-authors for their help in the preparation of this paper.

Conflicts of Interest: The authors declare that they have no known competing financial interests or personal relationships that could have appeared to influence the work reported in this paper.

References

1. Xu, Z. Research on Remnant Coal, Fully-Mechanized Mining Technology and Strata Behavior Regularity with the Old Mining Method. Ph.D. Thesis, Taiyuan University of Technology, Taiyuan, China, 2016.
2. Zhang, X. The Theory of Surrounding Rock Control and the Assessment Research of Recoverability in Thick Residual Coal Seam Remining Stope. Ph.D. Thesis, Taiyuan University of Technology, Taiyuan, China, 2015.
3. Zhang, X.; Gong, P.; Wang, K.; Li, J.; Jiang, Y. Characteristic and Mechanism of Roof Fracture Ahead of the Face in an LTCC Panel When Passing an Abandoned Roadway: A Case Study from the Shenghua Coal Mine, China. *Rock Mech. Rock Eng.* **2019**, *52*, 2775–2788. [[CrossRef](#)]
4. Xu, Y.; Ren, F.; Ahmed, Z.; Wang, K.; Wang, Z. Mechanical Characteristics and Damage Evolution Law of Sandstone with Prefabricated Cracks under Cyclic Loading. *Arab. J. Sci. Eng.* **2021**, *46*, 10641–10653. [[CrossRef](#)]
5. Xu, Y.; Ren, F.; Ahmed, Z.; Wang, K. Mechanical and Fatigue Damage Evolution Properties of Cracked Sandstone under Cyclic Loading. *Proc. Pak. Acad. Sci. A. Phys. Comput. Sci.* **2020**, *57*, 59–72. Available online: <https://paspk.org/wp-content/uploads/2020/09/ES-706.pdf> (accessed on 1 September 2023).
6. Wang, X.; Wang, E.; Liu, X.; Zhou, X. Failure mechanism of fractured rock and its AE behaviors under different loading rates. *Eng. Fract. Mech.* **2021**, *247*, 107674. [[CrossRef](#)]
7. Liu, Z.; Yang, S.; Bai, Z.; Huang, Y. Creep property and damage constitutive model of dioritic porphyrite under cyclic loading-unloading. *Chin. J. Eng.* **2022**, *44*, 143–151. [[CrossRef](#)]

8. Gao, S.; Cao, P.; Wang, S.; Pu, C. Improved nonlinear viscoelasto-plastic rheological model of rock and its correction of hardening coefficient of viscosity. *J. China Coal Soc.* **2012**, *37*, 936–943. [[CrossRef](#)]
9. Mishra, B.; Verma, P. Uniaxial and triaxial single and multistage creep tests on coal-measure shale rocks. *Int. J. Coal Geol.* **2015**, *137*, 55–65. [[CrossRef](#)]
10. Mansouri, H.; Ajalloeian, R. Mechanical behavior of salt rock under uniaxial compression and creep tests. *Int. J. Rock Mech. Min. Sci.* **2018**, *110*, 19–27. [[CrossRef](#)]
11. Andargoli, M.B.E.; Shahriar, K.; Ramezanzadeh, A.; Goshtasbi, K. The analysis of dates obtained from long-term creep tests to determine creep coefficients of rock salt. *Bull. Eng. Geol. Environ.* **2019**, *78*, 1617–1629. [[CrossRef](#)]
12. Fan, Q.; Li, S.; Gao, Y. Experimental study on creep properties of soft rock under triaxial compression. *Chin. J. Rock Mech. Eng.* **2007**, *7*, 1381–1385.
13. Wei, E.; Hu, B.; Li, J.; Cui, K.; Zhang, Z.; Cui, A.; Ma, L. Nonlinear Viscoelastic-Plastic Creep Model of Rock Based on Fractional Calculus. *Adv. Civ. Eng.* **2022**, *2022*, 3063972. [[CrossRef](#)]
14. Fahimifar, A.; Karami, M.; Fahimifar, A. Modifications to an elasto-visco-plastic constitutive model for prediction of creep deformation of rock samples. *Soils Found.* **2015**, *55*, 1364–1371. [[CrossRef](#)]
15. Liang, X.; Xue, X.; Wang, H.; Zhang, C. Damage creep characteristics of rock time-hardening. *J. Liaoning Tech. Univ. (Nat. Sci.)* **2013**, *32*, 509–512.
16. Song, Y.; Lei, S.; Liu, X. Non-linear rock creep model based on hardening and damage effect. *J. China Coal Soc.* **2012**, *37*, 287–292. [[CrossRef](#)]
17. Zhang, Q.; Yang, W.; Zhang, J.; Yang, C. Variable parameters-based creep damage constitutive model and its engineering application. *Chin. J. Rock Mech. Eng.* **2009**, *28*, 732–739.
18. Zou, J.; Zhao, T.; Fang, K.; Liu, X. Rock hardening and damage mechanism in step loading creep process. *J. Shandong Univ. Sci. Technol. (Nat. Sci.)* **2015**, *34*, 58–67. [[CrossRef](#)]
19. Cai, T.; Feng, Z.; Zhao, D.; Jiang, Y. A creep model for lean coal based on hardening-damage mechanism. *Rock Soil Mech.* **2018**, *39*, 61–68. [[CrossRef](#)]
20. Zhang, Z.; Song, Z.; Cheng, Y.; Huo, R.; Song, W.; Wang, K.; Wang, T.; Yang, T.; Liu, W. Acoustic emission characteristics and fracture response behavior of hard rock-like material under influence of loading rate. *Coal Geol. Explor.* **2022**, *50*, 115–124.
21. Ma, Q.; Tan, Y.; Liu, X.; Zhao, Z.; Fan, D.; Purev, L. Experimental and numerical simulation of loading rate effects on failure and strain energy characteristics of coal-rock composite samples. *J. Cent. South Univ.* **2021**, *28*, 3207–3222. [[CrossRef](#)]
22. Wang, C.; Wang, C.; Su, C.; Xiong, Z. Effects of different loading rates on Brazilian tension characteristics of limestone. *J. Min. Saf. Eng.* **2021**, *38*, 1036–1044. [[CrossRef](#)]
23. Wei, W.; Wei, A.; Duan, M. Effect of axial loading rate on mechanical and permeability properties of raw coal. *Saf. Coal Mines* **2021**, *52*, 39–46. [[CrossRef](#)]
24. Zhang, T.; Jing, C.; Wang, X.; Guo, H.; Zhang, L.; Pan, H. Experimental investigation of the effect of different loading rates on deformation characteristics of porous samples. *J. Min. Saf. Eng.* **2021**, *38*, 847–856. [[CrossRef](#)]
25. Zhang, J.; Yang, Y. Rock size effect and acoustic emission characteristics under the influence of loading rate. *China Min. Mag.* **2021**, *30*, 205–210.
26. Li, S.; Long, K.; Zhang, Z.; Yao, X. Cracking process and energy dissipation of sandstone under repetitive impact loading with different loading rates: From micro to macro scale. *Constr. Build. Mater.* **2021**, *302*, 124123. [[CrossRef](#)]
27. Wu, M. The effect of loading rate on the compressive and tensile strength of rocks. *Chin. J. Geotech. Eng.* **1982**, *4*, 97–106.
28. Wu, M.; Liu, Y. The effect of intermediate strain rates on mechanical properties of rock. *Rock Soil Mech.* **1980**, *2*, 51–58.
29. Guzev, M.; Riabokon, E.; Turbakov, M.; Kozhevnikov, E.; Poplygin, V. Modelling of the Dynamic Young's Modulus of a Sedimentary Rock Subjected to Nonstationary Loading. *Energies* **2020**, *13*, 6461. [[CrossRef](#)]
30. Marolt Čebašek, T.; Frühwirt, T. Investigation of creep behaviours of gypsum specimens with flaws under different uniaxial loads. *J. Rock Mech. Geotech. Eng.* **2018**, *10*, 151–163. [[CrossRef](#)]
31. Sun, L.; Yang, Z.; Tian, B.; Liu, Z.; Li, K. Study on the damage characteristics of rock burst at granite drift under different loading rates. *Min. Res. Dev.* **2017**, *37*, 44–49. [[CrossRef](#)]
32. Wang, Y.; Fu, J.; Wang, J. Study on uniaxial loading rate effect and fracture mesoscopic mechanism of mechanical properties of single fractured rock. *Min. Res. Dev.* **2020**, *40*, 66–74. [[CrossRef](#)]
33. Gattu, M. Effect of loading rate and material viscosity on fracture energy dissipation. *Mater. Today Proc.* **2023**, *in press*. [[CrossRef](#)]
34. Oh, S.-W.; Min, G.-J.; Park, S.-W.; Kim, M.-S.; Obara, Y.; Cho, S.-H. Anisotropic influence of fracture toughness on loading rate dependency for granitic rocks. *Eng. Fract. Mech.* **2019**, *221*, 106677. [[CrossRef](#)]
35. Xin, Y.; An, D.; Li, M.; Hao, H. Study of red-sandstone post-peak creep test in different loading rates. *J. China Coal Soc.* **2017**, *42*, 60–67. [[CrossRef](#)]
36. Wang, J.; Zhang, Q.; Song, Z.; Zhang, Y.; Liu, X. Mechanical properties and damage constitutive model for uniaxial compression of salt rock at different loading rates. *Int. J. Damage Mech.* **2021**, *30*, 739–763. [[CrossRef](#)]
37. Huang, P.; Zhang, J.; Damascene, N.J.; Wang, Z.; Li, M. Effect of loading rate on mechanical behavior of coal samples with initial damage accumulation. *Mech. Time-Depend. Mater.* **2021**, *26*, 309–322. [[CrossRef](#)]
38. Miyazaki, K.; Tenma, N.; Yamaguchi, T. Relationship between Creep Property and Loading-Rate Dependence of Strength of Artificial Methane-Hydrate-Bearing Toyoura Sand under Triaxial Compression. *Energies* **2017**, *10*, 1466. [[CrossRef](#)]

39. Li, J.; Lin, F.; Meng, L.; Zhang, H. Experimental research of varied loading method on creep of limestone. *Sci. Technol. Eng.* **2015**, *15*, 67–71+77.
40. Li, F.; Yang, J.; Liu, W.; Fan, Z.; Yang, Y. Effect of loading rate changing on the mechanical properties of mudstone under uniaxial compression. *Rock Soil Mech.* **2021**, *42*, 369–378.
41. Fan, Z. Study on Creep Characteristics of Mudstone Based on Loading Rate Effect. Master's Thesis, China University of Mining and Technology, Beijing, China, 2019.
42. Wang, Y.; Li, X.; Que, J.; Li, S. A porosity calculation method based on CT images and its application. *J. Hydraul. Eng.* **2015**, *46*, 357–365. [[CrossRef](#)]
43. Li, J.; Wang, D.; Kang, T. Algorithmic study on rock pore structure based on micro-CT experiment. *Chin. J. Geotech. Eng.* **2010**, *32*, 1703–1708.
44. Ahmed, Z.; Wang, S.; Hashmi, M.Z.; Zishan, Z.; Chengjin, Z. Causes, characterization, damage models, and constitutive modes for rock damage analysis: A review. *Arab. J. Geosci.* **2020**, *13*, 806. [[CrossRef](#)]

Disclaimer/Publisher's Note: The statements, opinions and data contained in all publications are solely those of the individual author(s) and contributor(s) and not of MDPI and/or the editor(s). MDPI and/or the editor(s) disclaim responsibility for any injury to people or property resulting from any ideas, methods, instructions or products referred to in the content.